NeuroImage **9,** 526–533 (1999)
Article ID nimg.1999.0435, available online at http://www.idealibrary.com on IDEAL®

Investigation of Low Frequency Drift in fMRI Signal

Anne M. Smith,*,[1] Bobbi K. Lewis,* Urs E. Ruttimann,† Frank Q. Ye,‡ Teresa M. Sinnwell,‡ Yihong Yang,* Jeff H. Duyn,* and Joseph A. Frank*

**Laboratory of Diagnostic Radiology Research, †National Institute on Alcohol Abuse and Alcoholism, and ‡National Institute of Mental Health, National Institute of Health, Bethesda, Maryland*

Received September 16, 1998

Low frequency drift (0.0–0.015 Hz) has often been reported in time series fMRI data. This drift has often been attributed to physiological noise or subject motion, but no studies have been done to test this assumption. Time series T_2^*-weighted volumes were acquired on two clinical 1.5 T MRI systems using spiral and EPI readout gradients from cadavers, a normal volunteer, and nonhomogeneous and homogeneous phantoms. The data were tested for significant differences ($P = 0.001$) from Gaussian noise in the frequency range 0.0–0.015 Hz. The percentage of voxels that were significant in data from the cadaver, normal volunteer, nonhomogeneous and homogeneous phantoms were 13.7–49.0%, 22.1–61.9%, 46.4–68.0%, and 1.10%, respectively. Low frequency drift was more pronounced in regions with high spatial intensity gradients. Significant drifting was present in data acquired from cadavers and nonhomogeneous phantoms and all pulse sequences tested, implying that scanner instabilities and not motion or physiological noise may be the major cause of the drift.

Key Words: **functional magnetic resonance imaging (fMRI); low frequency drift; BOLD; artifacts.**

INTRODUCTION

Several groups performing activation paradigms using the blood oxygenation level dependent (BOLD) contrast approach have reported low frequency drift (defined in this communication to be 0.0–0.015 Hz) in their time series data (1–4). Mattay *et al.* (3) reported that their time course data showed random low frequency drift with an approximate frequency of 0.0038 Hz and maximum amplitude of ~5% of the baseline signal intensity. Bandettini *et al.* (1) noted that the drifting was associated with large gradients of image intensity (i.e., tissue to bone interfaces). Genovese (5) reported that the low frequency drift was "typically smooth but could exhibit rapid localized changes and take quite varied forms." Turner *et al.* (4) proposed that the "drifts and shifts" seen in fMRI data may be due to long-term physiological shifts, movement related noise remaining after realignment, or from instrumental instability. The low frequency drift was usually removed by using linear models (1,2), low-order polynomial models (3), high-pass frequency filtering (4), or spline models (5).

Although the presence of low frequency drift is observed and reported in fMRI studies using different commercial brands of MRI scanners, the exact causes of this drift have not been extensively explored. Understanding the cause of low frequency drift is the first step towards correcting it, and if the low frequency drift can be eliminated from time series fMRI data, investigators would have more freedom in their choice of activation paradigms. In other words, they would no longer be limited to the boxcar on-off-on-off, etc., paradigms, which allow low frequency drift to be separated from true signal, but could use a simple off-on paradigm which would be useful for studies such as changes in blood flow in the brain before and after drug administration. We investigated the amount of low frequency drift present in data acquired from cadavers and phantoms (thus eliminating subject motion and physiological noise) and compared it to the amount measured in a normal volunteer.

METHODS

Cadavers

Three intact unfixed cadavers were obtained preautopsy from the Postmortem Section of the Laboratory of Pathology in the National Cancer Institute. Permission from relatives was obtained before scanning. Two cadavers were female (37 and 70 years old, cadavers 1 and 2, respectively). Cadaver 1 had died due to pneumonia and complications from Multiple Sclerosis, was transported via ambulance for 6 h, placed on the MRI scanner bed, scanned for >1 h (using a different protocol than that described in this paper), and finally was scanned using the protocol explained below. Ca-

[1] Current address: Neuroradiology, Cliniques Universitaires Saint Luc-UCL, Brussels, Belgium.

1053-8119/99 $30.00

daver 2 died from T-cell lymphoma, while the male cadaver (cadaver 3) was 67 years old and had died of multiple organ failure. All cadavers were dead for less than 24 h, cadavers 2 and 3 had been chilled at a temperature of 40°F overnight and all were scanned at room temperature.

Normal Volunteer and Phantoms

A 52-year-old male was scanned for all of the normal volunteer protocols. The subject laid quietly in the MRI scanner with eyes closed and performed no activation task. These studies were performed under an approved Intramural Review Board protocol at the National Institutes of Health.

Two types of phantoms were studied: a homogeneous and a nonhomogeneous phantom. The homogeneous phantom was a gel-filled spherical phantom from General Electric (Milwaukee, WI; Model No. 46-265826G3, description SNR head sphere) with T_1 = 800 ms and T_2 = 90 ms. The nonhomogeneous phantom was also from General Electric (Model No. 2131027-2, description DQA), which contained a solution of glycerin, sodium chloride, and deionized water. The phantom contained high spatial frequencies due to the presence of several bars, the letter A, and the logo of the manufacturer, and had T_1 values ranging from 123 to 1203 ms and T_2 values ranging from 89 to 939 ms. The phantoms were placed on the MRI patient bed, and the fMRI sequences were performed ≅ ½–1 h later.

Scanners

The fMRI data were acquired using two commercial 1.5 T MRI units (Signa Echospeed from General Electric Medical Systems, Milwaukee, WI), denoted as MRI units 1 and 2. MRI unit 1 was equipped with a General Electric magnet (S3), and MRI unit 2 was equipped with an Oxford magnet. Data were acquired from both scanners using a standard quadrature head coil. Each MRI unit was equipped with a different set of gradient amplifiers supplied by the manufacture and denoted as A (120 m · T/s slew rate, 2.3 G/cm maximum gradient strength) and B (120 m · T/s slew rate, 2.3 G/cm maximum gradient strength), with gradient amplifier B being smaller and more efficient. Both MRI units were equipped with identical, actively shielded gradient coil systems. MRI unit 1 had a passively shielded magnet while MRI unit 2 had no shielding around its magnet.

Data Acquisition

Anatomical images were acquired first using a fast spin echo sequence (24 cm field of view or FOV, TR = 3 s, effective TE = 34 ms). For the acquisition of the fMRI time series volumes, three different pulse sequences were used to determine if the low frequency drift in the time series data was pulse sequence dependent. Two of the sequences were in-house (spiral and echo planar imaging or EPI) (6,7), and the third was the manufacturer's EPI sequence. The spiral imaging sequence used the following parameters: TR (per single slice) = 55.6–62.5 ms, flip angle = 85°, TE = 35 ms, 32–36 slices 3.75 mm thick, 64 × 64 acquisition matrix, 24 cm FOV, acquisition time (acq) = 2 s/vol and 124 total acquisitions. The slices were acquired such that the entire brain was covered. The spiral sequence was used only on MRI unit 1 with both types of gradient amplifiers. The normal volunteer, all three cadavers and both phantoms were scanned using the spiral sequence. The custom developed EPI sequence and the manufacturer's EPI sequence used the following parameters: TE = 60 ms, TR (per single slice) = 1 s, 100 kHz sampling bandwidth, 4 slices 3.75 mm thick, 64 × 64 acquisition matrix, 24 cm FOV, acq = 4 s/vol and 124 total acquisitions. The same cadaver was scanned on MRI unit 1B and MRI unit 2A using the manufacturer's EPI sequence. The first 4 vol in all sequences were not used in the analysis to be sure that the signal had achieved steady-state magnetization. Therefore, data from two different MRI units, two different gradient amplifiers, three different pulse sequences, cadavers, a normal volunteer, and phantoms were all tested for the presence of low frequency drift.

Time Series Analysis

No normalization or volume registration was performed on any of the fMRI time series volumes. The average and variance were calculated for each time series on a voxel-by-voxel basis, and the corresponding average subtracted from the time series to prevent spectral leakage from high power at zero frequency into adjacent frequency bands because the time series data were later smoothed using a moving average filter. A mask was made from the average volume such that background voxels were not analyzed. The power density spectrum of the time series was calculated on a voxel-by-voxel basis, denoted by $\Psi_{i,j,k}(f_m)$, where i, j,k is the voxel location and $f_m = m/N\Delta t$ is the set of discrete frequencies, $m = 0, \ldots, N/2$, obtained by the FFT algorithm for a series of length $N = 120$ with sampling interval Δt = acq. To obtain a more reliable estimate of the spectrum, the power coefficients were smoothed by a rectangular moving average window of width $2M + 1$

$$\overline{\Psi}_{i,j,k}(f_m) = \frac{1}{2M+1}\sum_{q=-M}^{M}\Psi_{i,j,k}(f_{m+q}), \qquad m = M+1, \ldots N/2 - M - 1. \tag{1}$$

The hypothesis that the time series volumes were independent Gaussian-distributed noise was tested using a chi-square test for each smoothed power coefficient $\overline{\Psi}_{i,j,k}(f_m)$ (8). The power at frequency f_m was

considered significant when

$$\overline{\Psi}_{i,j,k}(f_m) > \sigma^2_{i,j,k} \cdot \frac{\chi^2(\alpha, \nu)}{\nu} \cdot \Delta t, \quad [2]$$

where $\sigma^2_{i,j,k}$ is the variance of the voxel time series, $\chi^2(\alpha, \nu)$ is the chi-square value for a given α (0.001), and $\nu = 2(2M + 1)$ is the degrees of freedom associated with the rectangular smoothing window. A smoothing window of 3 ($M = 1$) was selected, yielding $\nu = 6$ degrees of freedom (due to symmetry of the spectrum around $f = 0$) and 20 independent frequency bins. The probability of at least one bin in a single voxel time series (assuming the data was generated from a Gaussian distribution) being significant is 0.02 (α value of 0.001 times 20, the number of independent frequency bins tested). If the time series volumes were a sample of a Gaussian distribution with mean zero and variance $\sigma^2_{i,j,k}$, then the expected probability per voxel of having at least one significant bin is given by $P_{vox} = [1 - (1 - 0.001)^{20}] \approx 0.02$. Therefore, only 2.0% of the voxels tested should exceed the threshold given in Eq. [2] if the data were truly Gaussian noise.

The power spectrum was partitioned into three frequency bands: 0.0–0.015 Hz, 0.0167–0.099 Hz, and 0.1–0.5/acq Hz. These frequencies correspond to periods in the time domain of 66.7 $-\infty$ s, 10.1–60.0 s, and (2 $\times$ acq) $-$ 10 s. Therefore, low frequency drift was separated from artifacts that may occur in a medium frequency range (most activation paradigms are in this range with a period of 40–60 s) and from artifacts with power in a high frequency range such that may be associated with respiration and pulsating blood. A P value of 0.001/test was used to determine if the tested frequency was significantly different from a Gaussian distribution. Note that the P value is given per tested frequency, i.e., no correction was made for multiple tests in a given frequency band and hence the notation 0.001/test. The expected value for a given frequency band was calculated by multiplying the number of frequencies tested in the band by 0.001.

RESULTS

Time series fMRI studies were performed twice on the nonhomogeneous phantom and the normal volunteer using the spiral sequence, and both sets of data were analyzed to determine the percentage of voxels significantly different from Gaussian-distributed noise. The number of significantly different voxels in the two scans was always within $\pm$7.2% of each other. Further analysis used the average of the two scans.

The first slice in the phantom acquisitions using the spiral sequence was not used due to signal instabilities (the signal-to-noise ratio was much higher for this slice as compared to the others). Figure 1B shows the percentage change in the signal over time for a single voxel in a cadaver (see Fig. 1A for location of the voxel) and Fig. 1C is the power spectrum for this time series. Note that for this particular voxel located in the parietal cortex, only the very low frequencies were significantly different from white Gaussian noise.

In Table 1, the percentage of significant voxels from the different pulse sequences, MRI units and gradient amplifiers are shown divided into the three frequency bands. Note the relatively small percentage of significant voxels seen on data from the homogeneous phantom and that the values are much closer to the expected value had the images been white Gaussian noise only. Results from the normal volunteer demonstrate that only 1.9% (1.2% expected) of the brain voxels were significant in the high frequency band and that as much as 4.74% (0.67% expected) of brain voxels showed significance in the middle frequency band. The results from the cadaver with the same settings showed 0.56% significant voxels in the high frequency band and 0.70% in the middle frequency band. Note that gradient amplifier B always showed fewer significant voxels in the low frequency band for the corresponding settings as compared to gradient amplifier A.

Figure 2 shows the significant voxels from four central slices divided into the three frequency bands superimposed on the anatomical images for the homogeneous phantom (Fig. 2A), nonhomogeneous phantom (Fig. 2B), cadaver (Fig. 2C), and normal volunteer (Fig. 2D). Most of the significant voxels in the normal volunteer and cadaver data occurred in areas of high spatial anatomical variation (i.e., the large homogeneous white matter tracks showed fewer significant voxels compared to the convoluted gray matter). In the homogeneous phantom, the high and medium frequency significant voxels (red and green, respectively) did not show a distinct pattern in the spatial distribution, whereas the low frequency significant voxels (blue) were clustered near the edge of the phantom.

DISCUSSION

Time series fMRI volumes acquired from cadavers and nonhomogeneous phantoms surprisingly revealed significant amounts of low frequency drift, similar in magnitude to that of the normal volunteer. Low frequency drift was present in the processed images acquired from two different MRI units, two different gradient amplifiers, and all pulse sequences used (spiral, manufacturer's EPI, and custom developed EPI). The least amount of low frequency drift occurred in data acquired from a homogeneous phantom, where the drift occurred primarily at the edges of the phantom.

The low frequency drift observed in cadavers and the normal volunteer using sequential EPI or spiral imaging sequences was larger in regions with large spatial

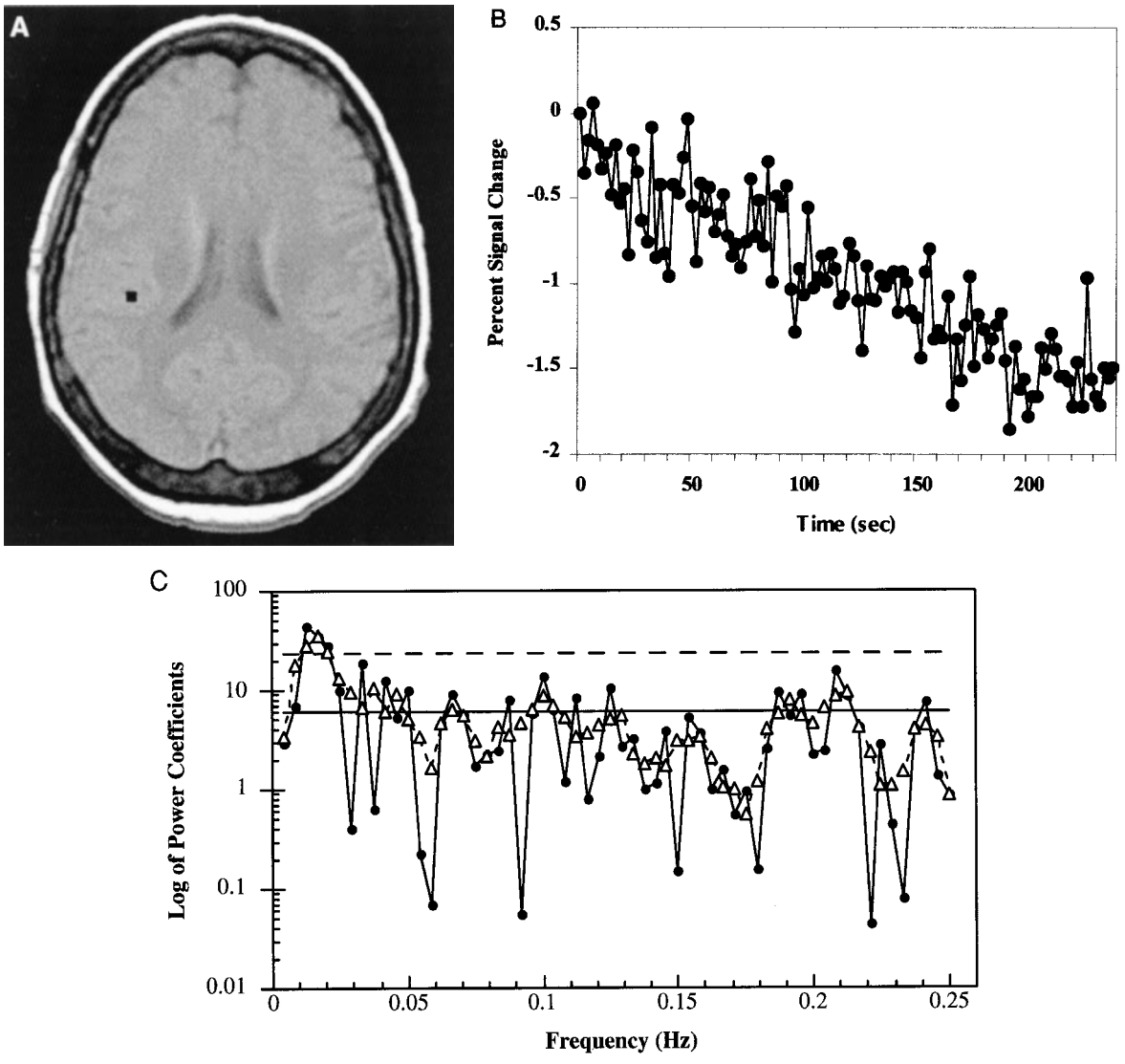

FIG. 1. (A) Location of single voxel (black square) in a cadaver used to generate the percent change in signal in series in B. (C) The log of the power spectrum coefficients (●) generated from the time series in B and the smoothed power coefficients (△). The solid line represents the variance of the selected voxel and the dotted line represents the upper limit of a 99.99% confidence interval assuming a Gaussian distribution. Note that the power in the low frequency range is significantly different from a Gaussian distribution for this particular voxel time series.

intensity gradient changes (i.e., gray-white matter interfaces) than in homogeneous regions (i.e., white matter). This observation agrees with that of Bandettini's *et al.* (1). Only 1.1% of the voxels in the homogeneous phantom showed significant low frequency drift (most significant voxels were near the central-lower left edge of the phantom), whereas cadavers, the normal volunteer and nonhomogeneous phantoms had 13.7–68.0% of their voxels with significant low frequency drift.

In the normal volunteer data, only 1.9% or less of the voxels showed significant power in the high frequency band (0.1–0.5/acq Hz). This was larger than the percentage observed in either the phantom or cadaver data but was not much larger than the expected value of 1.2%. Contamination of fMRI time series data from physiologic functions such as breathing or pulsating blood has been reported by several groups (9–11). Our sampling rate may not have been fast enough (2 s per volume during spiral acquisition) to sample these artifacts or they may have been aliased into the low or middle frequency bands. Note that two scans from the normal volunteer had greater than 4% (0.67% expected) of the voxels being significantly different from white noise in the middle frequency band (0.0167–0.099 Hz, the frequency of most activation paradigms), which could lead to false-positive activations.

The percentage of voxels that contained significant amounts of low frequency drift in data acquired from the normal volunteer was of the same magnitude as

TABLE 1

Percentage of Voxels with a Power Spectrum Significantly ($P = 0.001$/Test) Different from White Gaussian Noise for Data Collected from a Nonhomogeneous Phantom (Non-H Phan), Cadaver (Cad), Normal Volunteer (Norm Vol), and Homogeneous Phantom (Hom Phan) Using a Spiral, Manufacturer's EPI (M-EPI), or Custom Developed EPI (C-EPI) Sequence

Subject Sequence MRI unit	Non-H Phan Spiral 1A	Cad 1 Spiral 1A	Norm[a] Vol Spiral 1A	Cad 2 M-EPI 2A	Non-H[a] Phan Spiral 1B	Cad 3 Spiral 1B	Norm[a] Vol Spiral 1B	Hom[a] Phan Spiral 1B	Cad 2 M-EPI 1B	Cad 2 C-EPI 1B
Band 1	68.0	49.0	61.9	39.3	46.4	45.6	22.1	1.10	29.1	13.7
	(0.13)	(0.13)	(0.13)	(0.27)	(0.13)	(0.13)	(0.13)	(0.13)	(0.27)	(0.27)
Band 2	16.1	1.18	4.2	1.12	1.26	0.70	4.74	0.73	0.61	1.29
	(0.67)	(0.67)	(0.67)	(1.33)	(0.67)	(0.67)	(0.67)	(0.67)	(1.33)	(1.33)
Band 3	0.08	0.46	0.28	0.31	0.44	0.56	1.90	1.55	0.36	0.53
	(1.2)	(1.2)	(1.2)	(0.4)	(1.2)	(1.2)	(1.2)	(1.2)	(0.4)	(0.4)

Note. Band 1 represents frequencies in the range 0.0–0.015 Hz, Band 2 0.0167–0.099 Hz and Band 3 0.1–0.5/acq. The numbers in parentheses are the expected values if the images were only Gaussian-distributed noise.

[a] Average of two scans.

that from the cadavers or nonhomogeneous phantoms. These results imply that physiological noise or subject motion is not the major cause of low frequency drift. The most likely cause of the low frequency drift may be small changes in the magnetic field over time. When a slice from the first time volume of a cadaver or phantom was placed in a cine loop with the same slice from the last time volume, slight subvoxel nonrigid body movement was observed in all the data sets (of note: This subvoxel shift is not likely due to phantom or cadaver motion since both were secured firmly to the patient bed and the motion was a warping movement). Small local dynamic instabilities in the magnetic field could cause small misplacements of the voxels upon reconstruction, leading to partial volume effects that would be more apparent in regions with large spatial intensity gradient changes. Note that adjacent voxels can therefore display unrelated patterns of low frequency drift (i.e., signal intensity may increase then decrease in one voxel while in neighboring voxel the signal may only decrease with respect to time) which is often seen in fMRI time series data. To correct this problem, Birn *et al.* (12) proposed a method for correcting dynamic B-field artifacts by acquiring a B-field map with each acquired image volume. The B-field was then used to unwarp all the corresponding image volumes (13).

Possible causes of the changing magnetic field may be due to instabilities in the main B_o field or the gradient fields. Gradient system instabilities as reported by Edelstein *et al.* (14) may be due to small eddy currents that are caused by gradient field leakage around the ends of the shielding winding or by imperfect alignment of the inner and outer gradient windings. The eddy currents then produce time-dependent fields in the imaging region that are more noticeable in the hardware-demanding fMRI pulse sequences. Also, the gradient coils (and amplifier) may heat up throughout the course of an fMRI study. In this study, the experiments were performed with the same type of shielded gradient coils, two different gradient amplifiers, and 1.5 T magnets from different manufacturers. The results demonstrate a small difference in the percentage of significant voxels in the low frequency band between the two gradient amplifiers A and B, with amplifier B having fewer voxels with a power spectrum significantly different from Gaussian white noise for all imaged subjects. It is also worth noting that most commercial MRI units on the market today are not designed for the ultrafast pulse sequences used in fMRI, but rather for routine clinical imaging. Future generations of MRI units may be able to significantly reduce what appears to be hardware instabilities in fMRI data.

Other possible causes of the low frequency drift may be tissue/fluid shifting, establishment of thermal equilibrium, and damping of fluid flows. All effects listed will be present in cadavers, phantoms, and living subjects, but the establishment of thermal equilibrium may have been more pronounced in the two cadavers (cadavers 2 and 3) that had been chilled overnight and then scanned. The acquisition time of the EPI fMRI sequences were 8.3 min while for the spiral sequence it was 4.13 min. The amount of temperature change especially deep within the brain was likely negligible, yet significant low frequency drifting was still seen in all cadavers in the deep brain structures, even in cadaver 1 which had never been chilled and had been dead for >7 h.

We used cadavers in this study because we wanted to mimic as closely as possible the MR characteristics of humans yet not have any physiological noise or subject motion and they were available at our institution preautopsy. Cadavers have similar weight on the patient bed and load the MR coils in a similar manner as living subjects. The relaxation properties, proton density and magnetization transfer effects of unfixed intact

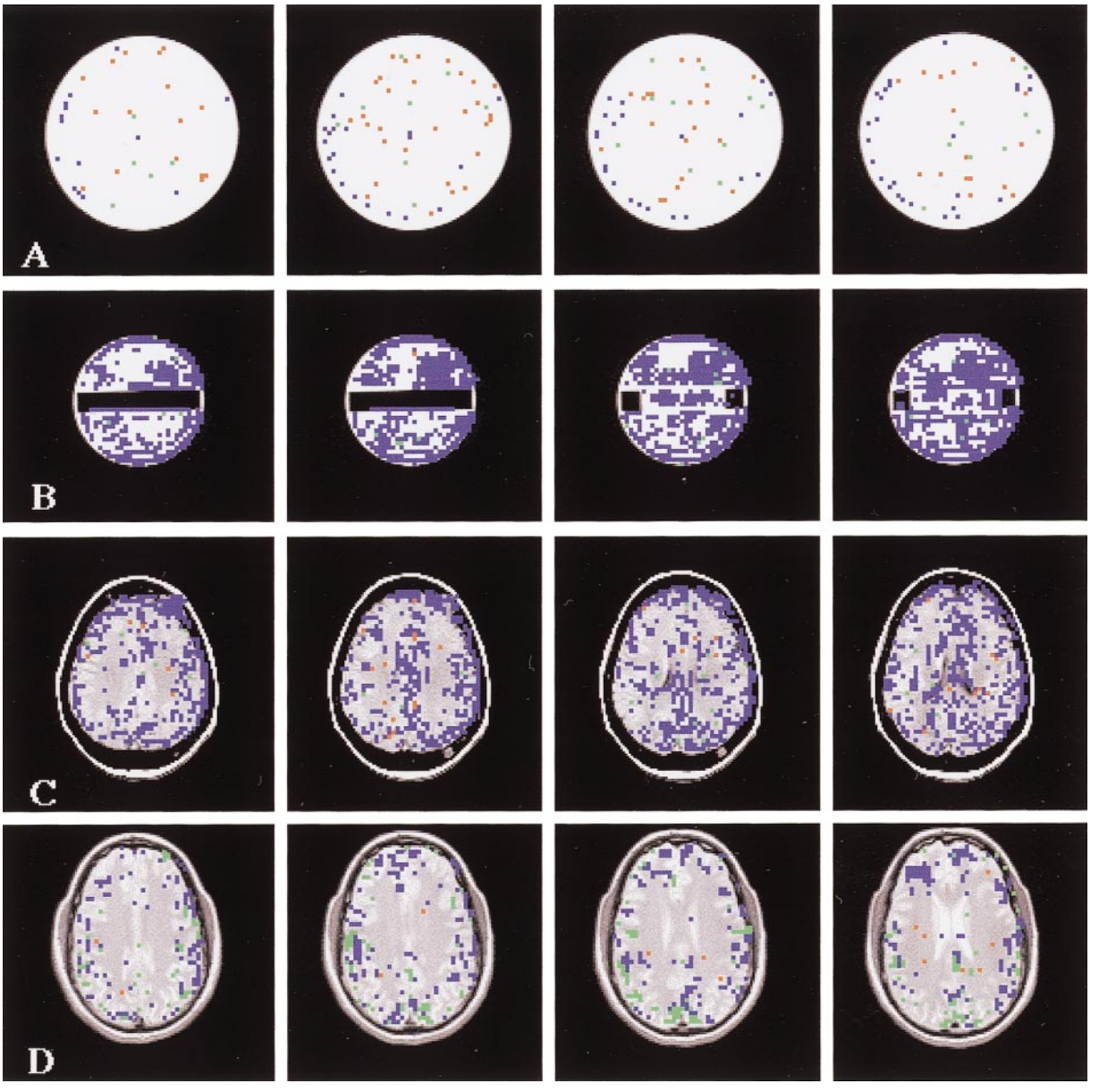

FIG. 2. Four different slices from the various subjects acquired with the spiral pulse sequence on MRI unit 1B (acq = 2 s). (A) Homogeneous spherical phantom. (B) Nonhomogeneous phantom. (C) Cadaver. (D) Normal volunteer. The colored voxels represent voxels that are significantly different from a Gaussian distribution for the three frequency ranges. Blue, 0.0–0.015 Hz; green, 0.0167–0.099 Hz; and red, 0.10–0.25 Hz.

cadavers are almost identical to that of a living subject (15,16), which can also be simulated using phantoms (17), but no standard or commercially available phantom with these properties currently exists. Cadavers also mimic the spatial frequencies found in living humans better than phantoms, which may explain why the time series data acquired from the nonhomogenous phantom in this study showed more low frequency drift than data from either the cadavers or the normal volunteer since the nonhomogenous phantom we used contained many edges and therefore had very high spatial frequencies.

Biswal and colleagues (18,19) demonstrated that low frequency fluctuations in time series fMRI data acquired from the resting human brain showed a high degree of temporal correlation ($P < 10^{-3}$) within and across associated regions of the sensorimotor cortex (18). In addition, they showed that the magnitude of these low frequency fluctuations was reversibly diminished during hypercapnia and that the spatial temporal correlation was also decreased (19). They hypothesized that the low frequency fluctuations are caused by spontaneous flow oscillations which are secondary to fluctuations in neuronal activity. Although our findings

seem to contrast those of Biswal *et al.*, significant differences in data analysis exist. First, they defined the low frequency drift to be <0.1 Hz, while our definition was <0.015 Hz. They also used a low-pass filter (cutoff 0.08 Hz) to eliminate fluctuations due to respiration and heartbeat while we performed no filtering. Low frequency drift commonly seen in fMRI time series data is therefore probably a combination of physiological noise and either scanner instabilities or thermal/settling properties of tissues.

The presence of low frequency drift means that single on-off activation paradigms cannot be used with time series fMRI volumes which can be limiting for certain types of studies such as before and after drug administration. In addition, there may be fewer true positive voxels detected when boxcar on-off-on-off-on, etc., paradigms are used since the high pass filtering often used to eliminate the low frequency drift may decrease the power of the true signal as well. As long as low frequency drift is present and cannot be corrected, activation paradigms should be designed with the highest possible fundamental on-off frequency such that the true signal can be separated from the low frequency drift. However, the highest possible frequency is limited by the hemodynamic response of the subject (6–8 s (20)), and most groups currently use a 20- to 30-s on or off epoch length. If low frequency drift is present in the data, some sort of correction for low frequency drift such as high pass filtering or polynomial fitting should be performed before the statistical analysis in order to increase the power of the statistical tests. However, if the low frequency drift could be corrected by using dynamic B-field mapping (12, see above), no low frequency filtering would be needed and the traditional boxcar activation paradigm would no longer have to be used.

It is possible to use a simple off-on activation paradigm in fMRI if such techniques as flow-sensitive alternating inversion recovery (FAIR) (21) or arterial spin tagging (AST) (22,23) are used. These techniques work by subtracting two adjacent time series fMRI volumes and analyzing the difference images. Since the low frequency drift was defined to have a maximum frequency of 0.015 Hz and the difference images represent a sampling of about 0.1 Hz (i.e., a single AST image is acquired in 4.7 s, therefore a difference image can be calculated every 9.4 s (23), but a difference image can be acquired as fast as every 4 s) very little signal change due to low frequency drift will be present in two adjacent images acquired using either the FAIR or AST techniques. Therefore, the difference images will reflect changes other than low frequency drift (i.e., blood flow changes, subject motion, etc). When we performed the same time series analysis that was used in this work on data acquired from a cadaver using these techniques, the FAIR data had 0.79% of its voxels in the entire frequency range which were significantly different from Gaussian white noise (1.13% expected), while AST had 0.5% (0.97% expected). Our group has been successful in using the AST technique with a 15-min off (subject viewing static) and 15-min on (subject viewing a movie) paradigm (A. M. Smith, unpublished data).

CONCLUSION

Time series data acquired using protocols sensitive to T_2^* changes associated with BOLD contrast showed that physiological noise and subject motion do not seem to be the main cause of the low frequency drift reported in fMRI time series data. The most likely cause of the drifting are slight changes in the local magnetic field due to scanner instabilities, thus causing a partial voluming effect in the reconstructed images which is more apparent in regions with large spatial intensity gradient changes.

ACKNOWLEDGMENTS

The authors thank Dr. David Kleiner, Mr. James Rainey, and Mr. Willie Young from the Postmortem Section of the Laboratory of Pathology in the National Cancer Institute for the use of the cadavers. The authors acknowledge the loan of the B gradient amplifier as part of a research agreement with General Electric Medical Systems. AMS was supported by a fellowship from the National Research Council.

REFERENCES

1. Bandettini, P. A., Jesmanowicz, A., Wong, E. C., and Hyde, J. S. 1993. Processing strategies for time-course data sets in functional MRI of the human brain. *Magn. Reson. Med.* **30:**161–173.
2. Bullmore, E., Brammer, M., Williams, S. C. R., Rabe-Hesketh, S., Janot, N., David, A., Mellers, J., Howard, R., and Sham, P. 1996. Statistical methods of estimation and inference for functional MR image analysis. *Magn. Reson. Med.* **35:**261–277.
3. Mattay, V. S., Frank, J. A., Santha, A. K. S., Pekar, J. J., Duyn, J. H., McLaughlin, A. C., and Weinberger, D. R. 1996. Whole-brain functional mapping with isotropic MR imaging. *Radiology* **201:**399–404.
4. Turner, R., Howseman, A., Rees, G., and Josephs, O. 1997. Functional imaging with magnetic resonance. In *Human Brain Function* (R. S. J. Frackowiak, Ed.), pp. 467–486. Academic Press, San Diego.
5. Genovese, C. R. 1997. A time-course model for fMRI data. In *Proc., ISMRM, 5th Annual Meeting,* p. 1669. Vancouver, B.C., Canada.
6. Yang, Y., Glover, G. H., van Gelderen, P., Venkata, S. M., Attanagoda, A. K. S., Sexton, R. H., Ramsey, N. F., Moonen, C. T. W., Weinberger, D. R., Frank, J. A., and Duyn, J. H. 1996. Fast 3D functional magnetic resonance imaging at 1.5 T with spiral acquisition. *Magn. Reson. Med.* **36:**620–626.
7. Yang, Y., Glover, G. H., van Gelderen, P., Patel, A. C., Mattay, V. S., Frank, J. A., and Duyn, J. H. 1998. A comparison of fast MR scan techniques for cerebral activation studies at 1.5 Tesla. *Magn. Reson. Med.* **39:**61–67.
8. Jenkins, G. M., and Watts, D. G. 1969. *Spectral Analysis and Its Applications.* Holden-Day, San Francisco.

9. Hu, X., Le, T. H., Parrish, T., and Erhard, P. 1995. Retrospective estimation and correction of physiological fluctuation in functional MRI. *Magn. Reson. Med.* **34:**201–212.
10. Wowk, B., McIntyre, M. C., and Saunders, J. K. 1997. k-space detection and correction of physiological artifacts in fMRI. *Magn. Reson. Med.* **38:**1029–1034.
11. Buonocore, M. H., and Maddock, R. J. 1997. Noise suppression digital filter for functional magnetic resonance imaging based on image reference data. *Magn. Reson. Med.* **38:**456–469.
12. Birn, R. M., Jesmanowicz, A., Cox, R. W., and Shaker, R. 1997. Correction of dynamic B_z-field artifacts in EPI. In *Proc., ISMRM, 5th Annual Meeting,* p. 1913. Vancouver, B.C., Canada.
13. Jezzard, P., and Balaban, R. S. 1995. Corrections for geometric distortion in echo planar images from B_o field variations. *Magn. Reson. Med.* **34:**65.
14. Edelstein, W. A., El Hamamsy, S-A., Schenck, J. F., Barber, W. D., and Gross, D. A. 1997. Calculation of time-dependent, gradient-induced axisymmetric eddy currents and fields. In *Proc., ISMRM, 5th Annual Meeting,* p. 1472. Vancouver, B.C., Canada.
15. Thickman, D. I., Kundel, H. L., and Wolf, G. 1983. Nuclear magnetic resonance characteristics of fresh and fixed tissue: The effect of elapsed time. *Radiology* **148:**183–185.
16. Newcombe, J., Hawkins, C. P., Henderson, C. L., Patel, H. A., Woodroofe, M. N., Hayes, G. M., Cuzner, M. L., MacManus, D., Du Boulay, E. P. G. H., and McDonald, W. I. 1991. Histopathology of multiple sclerosis lesions detected by magnetic resonance imaging in unfixed postmortem central nervous system tissue. *Brain* **114:**1013–1023.
17. Finelli, D. A. 1997. Magnetization transfer effects on T1-weighted three-dimensional gradient-echo MR images of a phantom simulating enhancing brain lesions. *Am. J. Neuroradiol.* **18:**147–159.
18. Biswal, B., Yetkin, F. Z., Haughton, V. M., and Hyde, J. S. 1995. Functional connectivity in the motor cortex of resting human brain using echo-planar MRI. *Magn. Reson. Med.* **34:**537–541.
19. Biswal, B., Hudetz, G. G., Yetkin, F. Z., Haughton, V. M., and Hyde, J. S. 1997. Hypercapnia reversibly suppresses low-frequency fluctuations in the human motor cortex during rest using echo-planar MRI. *J. Cereb. Blood Flow Metab.* **17:**301–308.
20. Friston, K. J., Holmes, A. P., Poline, J. B., Grasby, P. J., Williams, S. C. R., Frackowiak, R. S. J., and Turner, R. 1995. Analysis of fMRI time-series revisited. *Neuroimage* **2:**45–53.
21. Yang, Y., Frank, J. A., Hou, L., Ye, F. Q., McLaughlin, A. C., and Duyn, J. H. Multislice imaging of quantitative cerebral perfusion with pulsed arterial spin-labeling. *Magn. Reson. Med.* **39:**825–832.
22. Alsop, D. C., Maccotta, L., and Detre, J. A. 1997. Multi-slice perfusion imaging using adiabatic arterial spin labeling and an amplitude modulated control. In *Proc., ISMRM, 5th Annual Meeting,* p. 81. Vancouver, B.C., Canada.
23. Ye, F. Q., Smith, A. M., Mattay, V. S., Ruttiman, U. E., Frank, J. A., Weinberger, D. R., and McLaughlin, A. C. 1998. Quantitation of regional cerebral blood flow increases in prefrontal cortex during a working memory task: A steady-state arterial spin-tagging study. *Neuroimage* **8:**44–49.